Transient current pulses in rocket-extended wires used to trigger lightning

C. J. Biagi,[1] M. A. Uman,[1] J. D. Hill,[1] V. A. Rakov,[1] and D. M. Jordan[1]

Received 26 April 2011; revised 10 January 2012; accepted 27 January 2012; published 4 April 2012.

[1] We analyze current, electric field, and optical signatures of the sudden electrical breakdown processes (precursors) that occur at the top of the upward extending, grounded, Kevlar-covered copper wires used to artificially trigger lightning. For one launch, before the sustained upward positive leader initiated, we estimate that up to 10,000 precursors occurred (one every few hundred microseconds) with peak currents from 1 to more than 100 A. Luminosity at the wire tip was observed for 339 of 410 precursors examined in detail and, in seven cases, discharge channels developed to lengths of 3 to 8 m over times of several hundred microseconds. The measured propagation speeds of current pulses on the triggering wires were less than the speed of light, and decreased from about 2.8×10^8 m s^{-1} to about 2.3×10^8 m s^{-1} with increasing wire-top heights from about 80 m to about 340 m. The triggering wire and its grounding system are modeled as uniform transmission lines with model predictions that are consistent with the measured wire-base precursor current signatures. The modeling shows that (1) the characteristic impedance of the triggering wire, the ratio of the propagating precursor voltage pulse to its associated current pulse, is between 600 and 800 Ω; (2) the 25 m ground rod grounding impedance for the peak precursor current is about 100 Ω, while the DC grounding resistance is 20 Ω; and (3) the current reflection coefficient at ground for peak precursor current is ∼0.9.

Citation: Biagi, C. J., M. A. Uman, J. D. Hill, V. A. Rakov, and D. M. Jordan (2012), Transient current pulses in rocket-extended wires used to trigger lightning, *J. Geophys. Res.*, *117*, D07205, doi:10.1029/2011JD016161.

1. Introduction

[2] In rocket-and-wire triggered lightning, transient current pulses in the triggering wires are observed at ground before the development of a sustained upward positive leader from the wire tip. The current pulses are caused by electrical breakdown at the tip of wire where the electric field is significantly enhanced. The triggering wire is hypothesized to behave like a transmission line with the round-trip propagation time of the precursor pulse on the wire being greater than the pulse width. Current-pulse reflections are produced at the ground and at the wire tip. As a result, the current signature from a single precursor observed at ground is a sequence of pulses of alternating polarity and decreasing in amplitude during some tens of microseconds.

[3] The first description of current pulses preceding the inception of a sustained upward positive leader in triggered lightning was given by *Horii* [1982], who identified "pre-discharge" current pulses that were recorded at a 5 kHz sampling rate. Horii's current pulses occurred both as isolated events and in groups (two or more pulses occurring with intervals of several tens of microseconds) and had amplitudes between 0.1 A to 100 A. *Laroche et al.* [1988] observed current pulses and associated electric field pulses occurring prior to the inception of a sustained upward positive leader with intervals of some tens of milliseconds in isolation, or in groups, with the pulses within groups occurring about every 25 μs. Higher-magnitude current pulses exhibited damped oscillatory behavior, and the oscillation period increased with increasing wire length, leading *Laroche et al.* [1988] to hypothesize that the oscillations represented the transient response of the triggering wire. *Lalande et al.* [1998] observed current pulses exhibiting damped oscillatory behavior that were separated in time by 5 ms on average and lowered to ground several tens of microcoulombs. *Willett et al.* [1999] gave examples of similar damped oscillatory current pulses before the initiation of a sustained upward positive leader, along with corresponding damped oscillatory electric field signatures that resulted in a net electric field change owing to charge being lowered to ground. *Willett et al.* [1999] reported that the pulses occurred roughly every 10 ms, and sometimes occurred in groups with a pulse separation of 30 μs. The electrical breakdown that produces the current pulses preceding the inception of a sustained upward positive leader were first termed "precursors" by *Willett et al.* [1999].

[4] *Lalande et al.* [1998] speculated that the damped oscillatory current pulses are caused by aborted leader channels developing from the wire tip. The leader channels

[1]Department of Electrical and Computer Engineering, University of Florida, Gainesville, Florida, USA.

0148-0227/12/2011JD016161

stop elongating when the electric field intensity above the leader channel is below the level required to sustain the leader's propagation. *Biagi et al.* [2009] presented images of two luminous channels at the triggering wire tip that were time correlated with two wire-base current pulses, confirming that the observed current pulses were associated with aborted leader channels at the wire tip. The aborted leader channels had observed lengths of 1.5 and 8 m at heights of 128 and 158 m above ground level, respectively, and had luminosity similar to that of the sustained upward positive leader. *Biagi et al.* [2009] noted that no luminosity could be detected in association with several other precursor current pulses in the same triggering wire launch, perhaps indicating that lower-luminosity processes such as corona or corona streamers produce at least some of the observed current pulses.

[5] The precursor current signature that is measured at ground contains information regarding the electrical parameters of the triggering wire, including the charge on and around the wire and the grounding conditions. Precursors, and the resultant propagation of the current pulses on the triggering wire, are unique phenomena that can also provide useful experimental data on current propagation and attenuation on vertical conductors of finite length. In this paper, we first examine the wire-base current, electric field, and optical signatures of precursors. Then, using measurements of precursors and a distributed circuit transmission line model, we show that the triggering wire acts like a transverse electromagnetic wave guiding structure, and we attempt to infer the salient electrical parameters of the triggering wire system and its ground termination.

[6] The paper's organization is as follows. After describing the experiment in section 2, we present new observations and measurements of precursor luminosity, currents, and remote electric fields in section 3. In section 4, we analyze the wire-base precursor current measurements to estimate the propagation speeds of current pulses on the triggering wire and the current-pulse attenuation due to propagation losses and reflections at both ends of the triggering wire. In section 5, we describe our transmission line model and compare its predictions with our measurements. A brief discussion of our observations and modeling is found in section 6.

2. Experiment

[7] The experiment was performed during the summer of 2009 at the International Center for Lightning Research and Testing (ICLRT) located in north-central Florida, a facility that is operated jointly by the University of Florida and Florida Institute of Technology. The experimental setup is similar to that described by *Biagi et al.* [2011]. Rockets trailing grounded triggering wires were launched from a 3 m launch tube assembly on top of an 11 m high launch tower located near the center of the experimental site. The triggering wires were 0.2 mm diameter copper that were Kevlar reinforced. The rocket (and wire-top) heights were tracked with high-speed video cameras (described later in this section). Straight, vertical, and 2.5 cm wide copper "shield braid" (referred to as the ground lead) 11 m in length connected the launch tubes located on top of the launch tower (and hence the bottom of the triggering wire) to the grounding system, which was a buried, 16 mm diameter, 25 m length vertical ground rod. The measured low-frequency, low-current grounding resistance of the 25 m ground rod was about 20 Ω [*Crawford et al.*, 2001]. Currents in the triggering wires were measured on the launch tower beneath the launch tubes (at the top of the ground lead) using a non-inductive current shunt having a constant resistance of 1 mΩ from DC to 8 MHz, and, in some launches, a Pearson coil (current transformer) with a flat response over a frequency range 8 Hz to 5 MHz. It is shown in section 5 through modeling that placing the current measurement between the 11 m ground lead and the triggering wire yields virtually the same waveform signatures as would be obtained if the measurement were made at the bottom of the ground lead, just above the buried ground rod.

[8] Remote electric fields were measured using a capacitively coupled, flat-plate sensor installed flush with ground [*Jerauld*, 2007], and located 156 m north of the launch tower (henceforth referred to as "E2"). The E2 sensor was designed to measure field intensities ranging from about 1 to 100 V m^{-1} with a 3 dB upper frequency response of 3 MHz and a decay time of 10 ms to 1/e level for a step function input. Exposing the flat-plate antenna to rain saturated the sensor electronics due to their high sensitivity. A thin, rigid plastic dome was placed over the sensor to shield it from rain and prevent it from saturating, but doing so apparently enhanced the amplitude sensitivity by about 29% (see *Biagi et al.* [2011] for details on the electric field sensor calibration). Note that the electric field data presented here are not altered to account for this enhancement since no results presented in this paper depend on the amplitude, only the waveshape. Both current measurements and the E2 measurement were bandwidth limited to 3 MHz (low-pass filtered), and were digitized at a 10 MHz sampling rate with 12 bit amplitude resolution.

[9] In this study, a positive electric field at ground corresponds to the electric field vector pointing upward (physics sign convention). Positive current and negative electric field change at ground correspond to the removal of negative charge from or the deposition of positive charge in the atmosphere.

[10] A Vision Research Phantom V7.3 high-speed video camera operated at a distance of 440 m west of the launch tower with a framing rate between 5 and 10 thousand frames per second (kfps) with 14 bit gray scale resolution. The lens focal length was either 20 or 24 mm, which provided spatial resolutions of 0.48 or 0.40 m per pixel, respectively. The effective vertical field of view (FOV) of the camera was from ground to about 320 m and 275 m above ground level (AGL). The horizontal FOV was about 100 m centered on the launch tower. All heights given herein are AGL. The high-speed video, wire-base currents, and electric field measurements were synchronized using GPS timing.

3. Data and Observations

[11] We have examined the luminosity, wire-base current, and electric field signatures for 410 precursors in 15 wire launches, some of which are presented in this section. We begin with describing the luminosity that was often observed at the wire tips in association with the precursors. Next, we present examples of the wire-base current and electric field

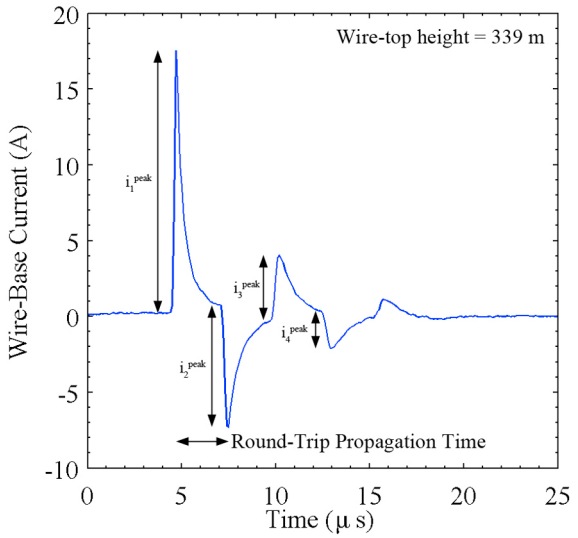

Figure 1. Current signature of a precursor in which the first current pulse, and subsequent current pulses resulting from reflections from the wire base and wire top, are clearly separated in time and are easily distinguishable. Peak amplitude measurements that are used in the analysis of section 4.2 are identified along with the round-trip propagation time (peak-to-peak time). This is precursor 3 that is modeled in section 5.

signatures of precursors from two separate wire launches, and we describe the variability in precursor behavior that was observed.

3.1. Luminosity Associated With Precursor Current Pulses

[12] Of the 410 precursor current signatures examined, 339 (83%) were correlated with observations of luminosity at the wire tip in high-speed video recordings that varied from a meter or so of dim, diffuse glow that often appeared fan-shaped, to distinct leader channels of several meters length. In seven cases, leader channel extended from the wire tip in two consecutive high-speed video frames (or a time of a few hundred microseconds) to a maximum length from 3 to 8 m. Each observation of leader channel corresponded to "bursts" of precursors (2 to 7 precursors occurring in rapid succession within tens of microseconds of each other) indicating that the aborted leaders developed stepwise. The type of luminosity that was observed, or lack thereof, certainly depended on the general visibility conditions (e.g., background light, rain) as well as the camera frame rate and lens aperture. Two photographs of typical precursors are found in the work of *Biagi et al.* [2009, Figure 2].

3.2. Precursor Current and Electric Field Signatures

[13] Figure 1 presents an example of the wire-base current for a precursor observed when the wire-top height was 339 m, for which the current pulse width was clearly shorter than the round-trip propagation time (the time between successive peaks). As a result, the current pulses produced by successive reflections at the wire base and wire tip are easily distinguishable, and measuring the amplitudes and timing of the precursor signature features is straightforward. The first peak of the damped oscillatory signature measured at the wire base is the superposition of the current pulse that was generated at the wire tip, after having traveled down the wire, and a reflected current pulse of the same polarity from the approximately short-circuit termination at the ground rod. The reflected current pulse propagates up the wire to the wire tip, where it encounters approximately open-circuit conditions, and an opposite-polarity (negative) current pulse reflection is produced that travels down the wire to ground. The second peak of the damped oscillatory signature measured at the wire base is the superposition of the negative current pulse and another ground-reflected current pulse (that is also of negative polarity). This sequence of reflections repeats, with the current polarity reversing with each wire-tip reflection, resulting in the oscillatory nature of the wire-base measurement. The energy losses associated with the wire (primarily resistance and corona leakage current) and imperfect reflections at the wire tip and at the ground attenuate the current, and hence damp the oscillatory current-

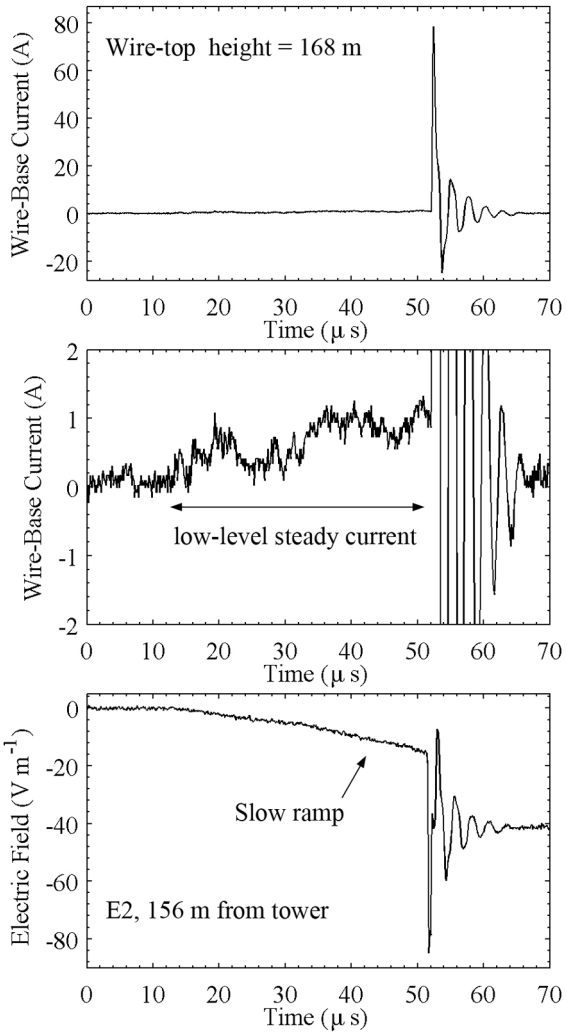

Figure 2. Signatures of wire-base current shown at (top) full scale and (middle) ±2 A scale and of (bottom) electric field for a precursor that exhibited an initial low-level, steady current, and corresponding electric field ramp.

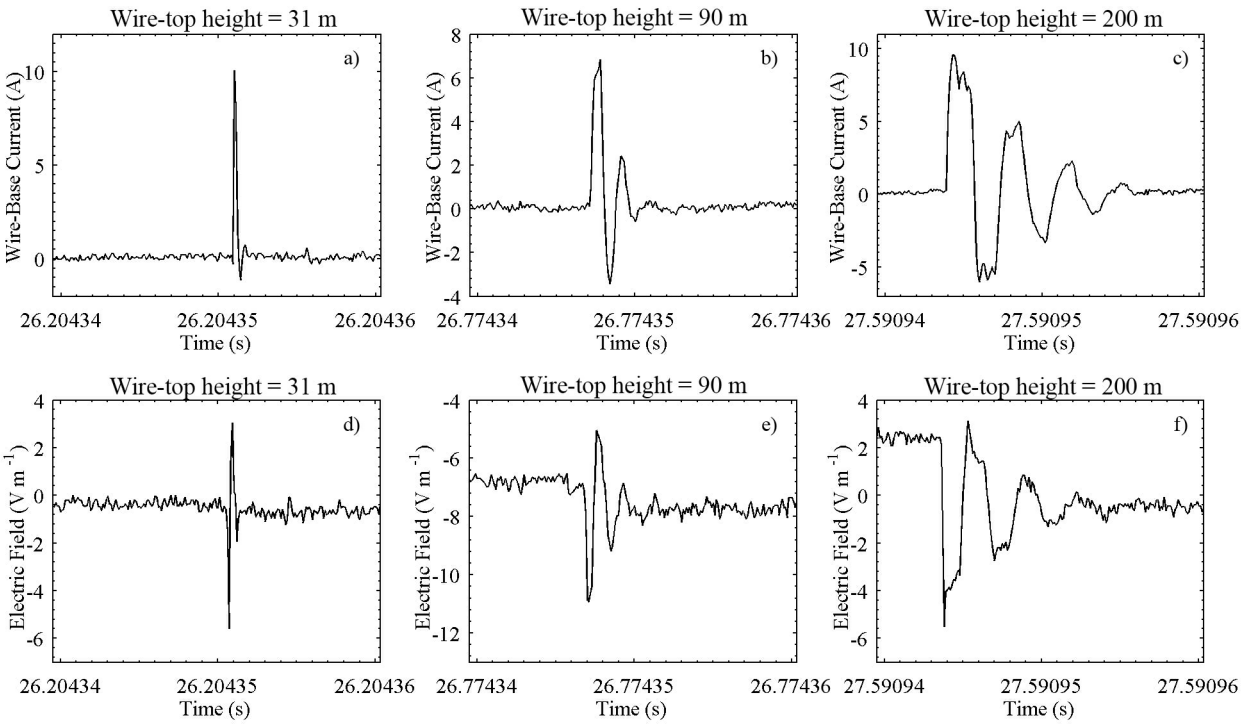

Figure 3. (a–c) Wire-base current at 156 m and (d–f) respective electric field measured by E2 for three precursor signatures (one in each column) from event UF0911. Each plot is at 20 μs full scale. The wire-top heights were about 31 m, 90 m, and 200 m for Figures 3a and 3d, Figures 3b and 3e, and Figures 3c and 3f, respectively. As the wire-top height increased, the number of current reflections increased, and the pulses increased in width.

pulse signature observed at ground. The shape of each successive pulse appears increasingly distorted, or "smoothed," indicating that there is some frequency dependence in the process.

[14] Figure 2 presents the current and electric field signatures for a precursor that occurred at a wire-top height of 168 m (about half that of the precursor shown in Figure 1). Note that the individual pulses for the precursor signature of Figure 2 are not well separated in time. A low-level, steady current flows for about 40 μs and reaches a level of about 1 A before the much larger damped oscillatory signature begins. A slow ramp in the electric field begins with the steady current flow, and ends when the damped oscillatory signature begins. These features were observed in 126 (31%) of the 410 precursors analyzed. It is certainly possible that these features always occur but are sometimes below the noise floor of the measurements (a current level of about 1 A and a field change of about 1 V m^{-1}) and thus are undetectable.

[15] The precursor signatures presented in Figures 1 and 2 are relatively simple in shape. The majority of the precursor signatures analyzed displayed more complexity in the pulse structure, such as two or more peaks, nonmonotonic rising and falling edges, and/or irregular oscillations, indicating a more complex electrical breakdown at the wire tip. The current pulse reflections in most precursor signatures overlapped; that is, they were not clearly separated in time. In addition, since the pulse structure is distorted more with each successive reflection cycle, distinguishing features, such as multiple peaks (for example, the precursor that occurred at a wire-top height of 200 m in Figure 3), are often lost, typically by the fourth pulse. Precursors tended to occur in bursts more frequently with increasing wire-top height. There was no obvious relationship between the height at which the precursors occurred and the precursor features, such as low-level steady current, on pulse shape.

[16] Figure 3 shows how the precursor signatures change as the triggering wire extends with three examples of precursor signatures in wire-base current and electric field from wire launch UF0911 (the 11th launch of 2009) at the beginning (26.20435 s), in the middle (26.77435 s), and just before the upward positive leader (27.59095 s) when the wire-top heights were 31 m, 90 m, and 200 m, respectively (the full record for Launch UF0911 is shown in Figure 4). As the wire-top height increased, the number of current reflections increased, and the pulses increased in width. Note that for the precursor that occurred when the wire-top height was 200 m, the initial current pulse has a multipeak structure that is lost by the fourth pulse.

3.3. Precursor Rates

[17] Precursors occur at different rates in different wire launches. As an example, we present data for two launches within a time of about 18 min in which precursors occurred at significantly different rates, even though the wires were extended upward beneath the same thunderstorm at similar extension rates, and initiated sustained upward positive leaders at about the same heights. As can be seen in Figure 4, precursors in launch UF0911 occurred quasiperiodically (with a periodicity that was regular, but with slightly

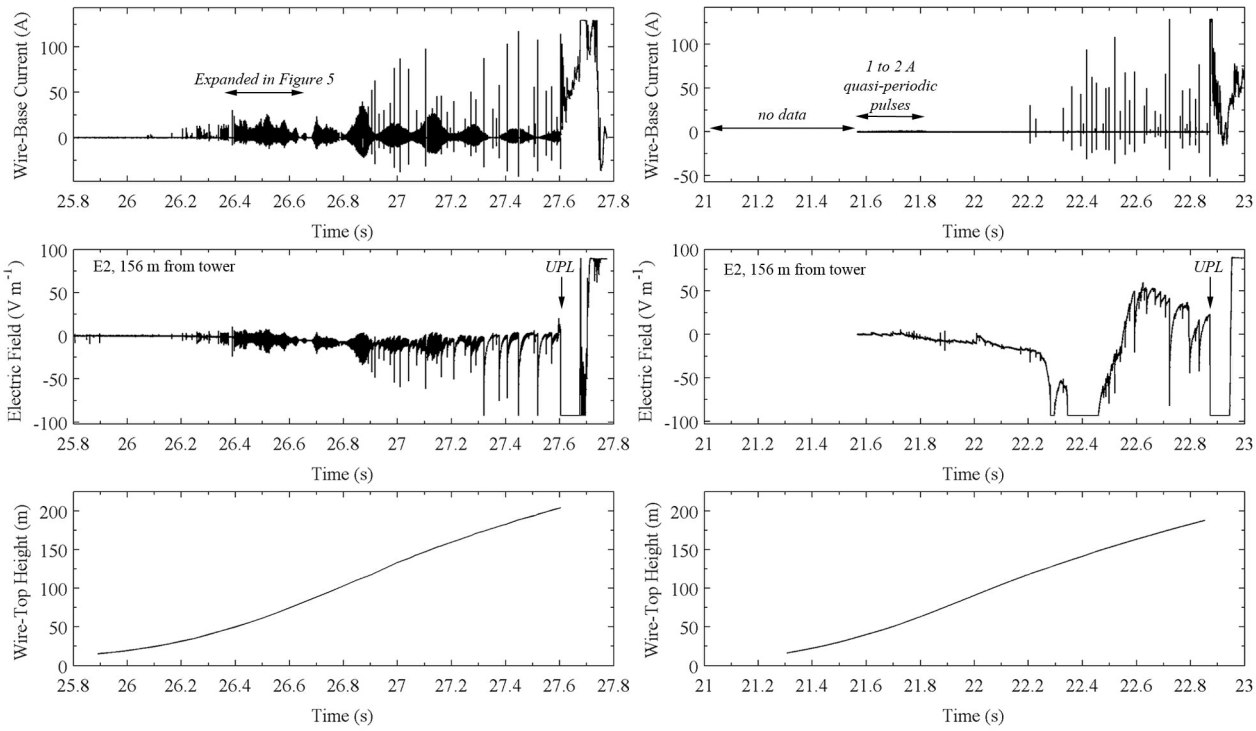

Figure 4. (top) Wire-base current, (middle) electric field, and (bottom) wire-top height for wire launches (left) UF0911 and (right) UF0912 on a 2 s time scale. The wire-base current and electric field measurements saturate at about 125 A and ± 85 V m^{-1}, respectively. Note that no data were recorded before about 21.55 s for UF0912. The sustained upward positive leader of UF0911 began at time 27.604 s, when the wire-tip height was about 234 m. The sustained upward positive leader of UF0912 began at time 22.85 s, when the wire-tip height was about 190 m. The solid "envelope" in the current and electric field records for UF0911 that varies with a period around 200 ms is composed of thousands of individual pulses that are not resolvable on this time scale. Some of these pulses are discernable in the time-expanded view of the record from 26.35 to 26.65 s (as identified by the double-ended arrow in Figure 4) shown in Figure 5. Note that for UF0912, much of the recorded electric field change from time 21.6 to 22.4 s is due to separate and unrelated lightning process (signatures corresponding to distant preliminary breakdown and cloud discharges are evident when the field record is examined on an expanded time scale).

different times from precursor to precursor) throughout the wire ascent, generally every several hundred microseconds to a few milliseconds. On the basis of the total time during which precursors occurred in launch UF0911 (about 1.4 s), we estimate that between 5,000 and 10,000 individual precursors occurred during the wire ascent. In the second wire launch (UF0912), shown in Figure 4, precursors occurred quasiperiodically only during a 250 ms interval for wire-top heights from about 30 m to 60 m, followed by a 380 ms interval with no measurable current in the wire, and then 41 precursors without obvious periodicity. The quasi-static electric field at ground level [*Biagi et al.*, 2011] when the two wires were launched was similar, 5.7 and 5.1 kV m^{-1} for launches UF0911 and UF0912, respectively, and both wire extensions produced a field reduction at ground of about -2.7 kV m^{-1}.

[18] For UF0911, the precursor current pulses began at about 26.1 s, when the wire tip was at a height of about 30 m AGL. Note that the pulses in electric field before time 26.1 s were not produced by current in the wire. Between times 26.1 and 26.3 s, the current pulses occur sporadically and are unipolar, while the corresponding electric field pulses are bipolar. The pulses begin occurring quasiperiodically just after time 26.3 s. Figure 5 presents a 300 ms expanded view of pulses from 26.35 s to 26.65 s showing that the amplitude envelope of the current pulses exhibits somewhat periodic variations, and that the current pulses occur less frequently when the pulse amplitudes are larger, a general feature of all the launches. After time 26.8 s in UF0911, the amplitude envelope of the current pulses varies with more distinct periodicity. At time 26.9 s, larger current pulses and pulse bursts begin occurring, somewhat randomly, with magnitudes many times that of the pulses occurring quasiperiodically.

3.4. Negative-Polarity Precursors

[19] In one launch (UF0901), made when the ground-level electric field was -4.5 kV m^{-1} indicating that predominately positive charge was overhead, we observed negative-polarity precursor signatures in current and electric field occurring quasiperiodically every several hundred microseconds in a manner similar to those from UF0911 (see section 3.3). These observations are presented in Figure 6. Launch UF0901 was not recorded in video, so there was no

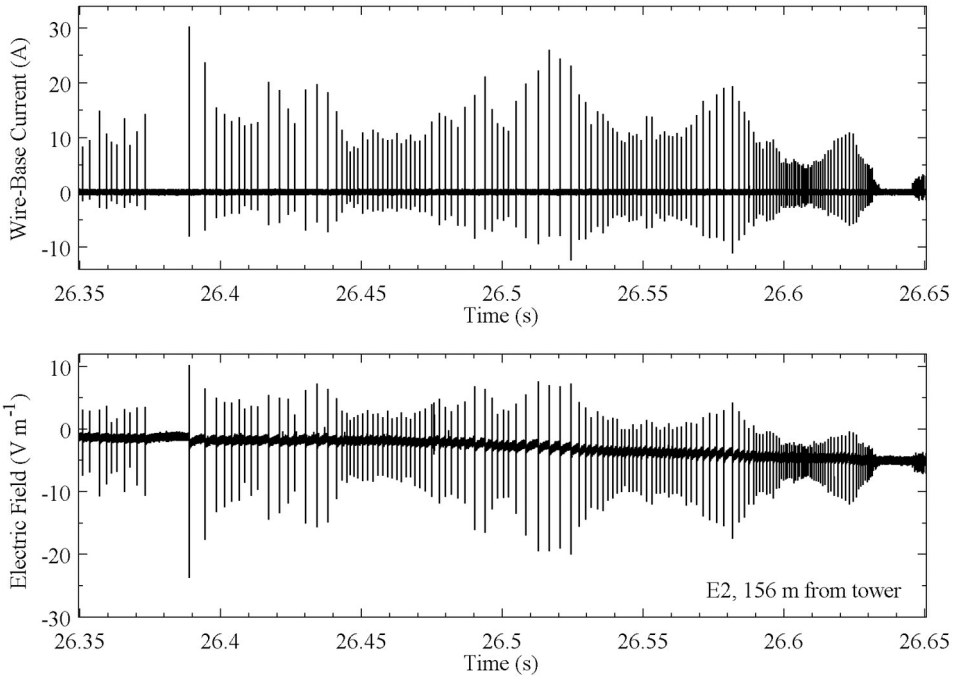

Figure 5. An expanded view of (top) wire-base current and (bottom) electric field precursors of UF0911 viewed at 300 ms full scale. Pulses occur less frequently when the pulse amplitudes are larger.

measurement of the wire-top height versus time or observations of luminosity corresponding to the precursors. However, on the basis of the time when the rocket was launched and the modeled trajectory of *Biagi et al.* [2011], we estimate that the precursor signatures presented in Figure 6 occurred when the wire-top height was somewhere between 75 and 125 m. The observed negative-polarity precursors do not appear much different in rate and shape from positive-polarity precursors. The negative-polarity precursors occurred at a rate of about one every 1 ms, and

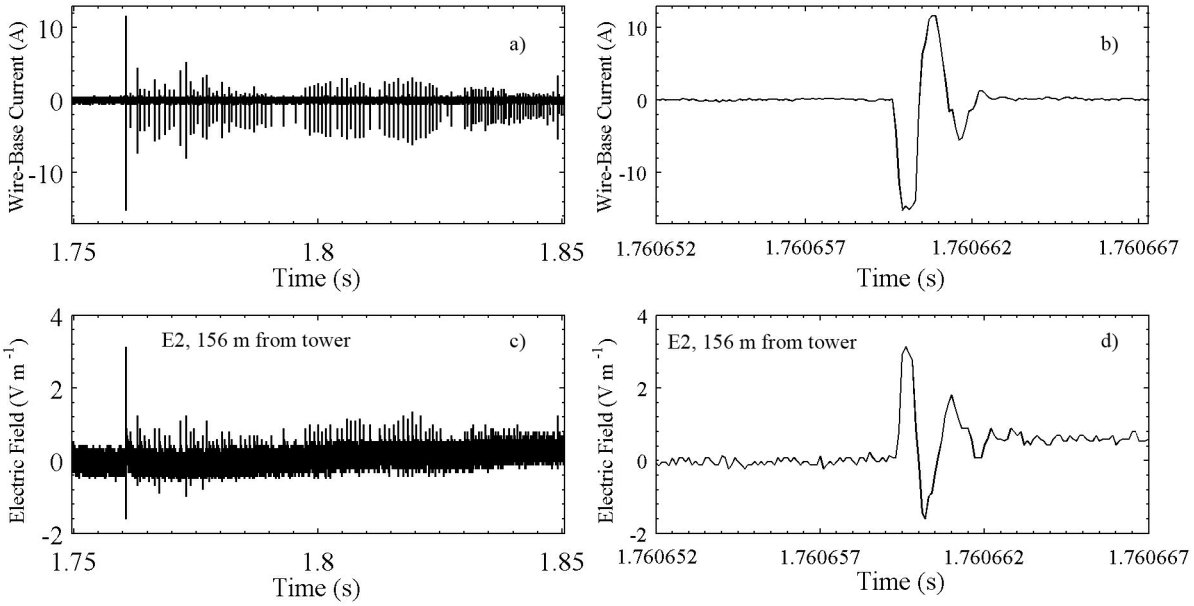

Figure 6. (a and b) Wire-base current and (c and d) electric field signatures of negative-polarity precursors during wire launch UF0901. Figures 6a and 6c show the precursor signatures on a 100 ms time scale. Figures 6b and 6d show, on a 15 μs time scale, the largest precursor signature that occurred at time 1.76066 s. We estimate that these precursor signatures occurred when the wire-top height was somewhere between 75 and 125 m (see section 3.4).

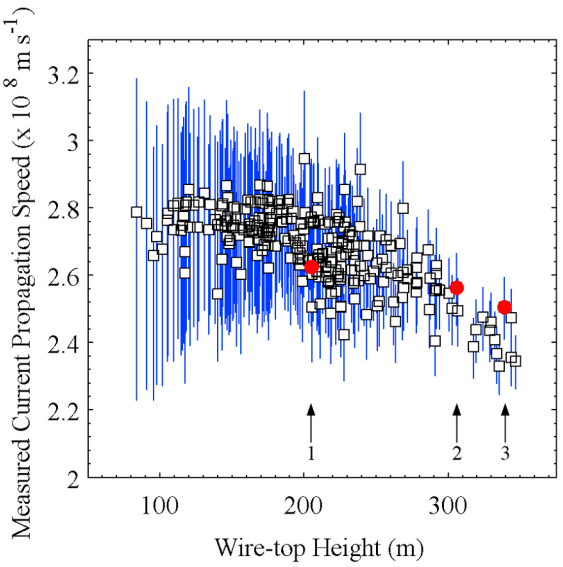

Figure 7. Scatterplot showing the measured current propagation speeds (the ratio of wire-top height to one half of the average peak-to-peak times) versus wire-top heights for 271 precursors. The blue vertical lines show the margins of error that result from the peak time measurement's having a timing uncertainty of 200 ns (±100 ns). The data points for precursors 1, 2, and 3 that are modeled in section 5 are plotted as red circles and are pointed to by black arrows numbered 1, 2, and 3. Note that the vertical scale starts at 2×10^8 m s^{-1} and that many data points overlay.

generally had peak currents of several amperes and electric field changes of a few volts per meter.

4. Analysis

[20] This section contains analysis of measured precursor current signatures. First, the propagation speeds of the current pulses along the wire are measured. Then, information is developed from which the apparent attenuation of the current pulses owing to propagation losses and imperfect current reflections with each round trip on the wire can be estimated and compared to our model (see section 5.3). Finally, the charges in the first current pulse and in the entire precursor current signature, as measured at the wire base, are compared.

4.1. Propagation Speed

[21] The propagation speeds of current pulses on the triggering wire are found from wire-base current measurements by dividing the wire-top height by one half of the average of the times between the successive peaks (round-trip propagation times) for the first six peaks. For most precursors, the peak-to-peak times were equal within 200 ns, or 2 sample points. There were 271 precursor signatures with single-peaked pulses that were not saturated and hence suitable for current-pulse propagation speed measurement. The speeds of the current pulses for these precursors are plotted versus wire height in Figure 7. There is uncertainty of at least 200 ns (one sample point time for each peak-time measurement) in the round-trip propagation time that introduces a margin of error in the current-pulse speed calculations (shown as blue bars in Figure 7). The top and bottom of the blue error bars are the computed speeds if 200 ns is subtracted or added, respectively, from the round-trip propagation time. Note that for greater wire lengths, the round-trip propagation time is greater, and the 200 ns timing uncertainty is less significant (explaining why the blue error bars decrease with increasing wire lengths). The current-pulse propagation speed is roughly between 2.7×10^8 and 2.8×10^8 m s^{-1} (disregarding the 200 ns uncertainty) for wire-top heights from 80 m to 200 m. The speed decreases for larger wire-top heights by about 20%, to as low as about 2.3×10^8 m s^{-1} for a wire-top height of 340 m. The measured speeds of three specific precursors used in the modeling (see section 5) are identified in Figure 7. None of the six wires studied here exhibited a tilt angle of more than a few degrees or had a significant curvature. We estimate that the wire tops did not deviate horizontally from the launch tower more than 10 m.

4.2. Precursor Charge and Current

[22] The precursor signature in Figure 1 is one of 19 signatures in which the starting point of the successive pulses were clearly distinguishable so that pulse amplitudes could be measured accurately. For these 19 precursor signatures, which occurred at wire-tip heights between 135 m and 340 m, the peak amplitudes of the first four current pulses, i_n^{peak} where n = 1, 2, 3, 4 (as identified in Figure 1), were measured. Figure 8 is a scatterplot of the computed ratios i_2^{peak}/i_1^{peak}, i_3^{peak}/i_2^{peak}, i_4^{peak}/i_3^{peak} versus wire-top height for the 19 precursors signatures. The ratios were distributed from 0.45 to 0.75, and the arithmetic mean of all the ratios was 0.60. There was no apparent relationship between ratios of current peaks and wire-top heights.

[23] There was a clear relationship between the charge in the first current pulse, Q_1, and the total charge delivered to ground by the end of the entire precursor current signature, Q_{Total}. These charges were determined by computing the time integral of the current from the beginning of the precursor signature to: (1) the beginning of the second pulse for Q_1, and (2) the point when the current attenuates below the measurement noise floor for Q_{Total}. The charges Q_1 and

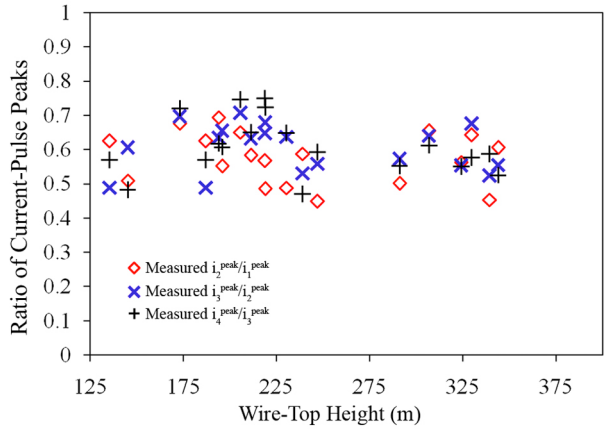

Figure 8. Scatterplot of the current-peak ratios i_2^{peak}/i_1^{peak}, i_3^{peak}/i_2^{peak}, and i_4^{peak}/i_3^{peak} for 19 measured precursor current signatures (see section 4.2).

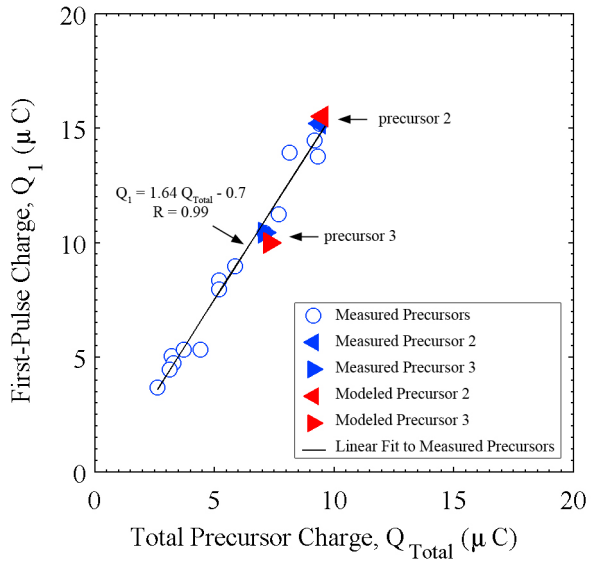

Figure 9. Scatterplot of the charge transferred to ground during the initial precursor current pulse versus the total charge transferred to ground by the end of the precursor current signature for 15 measured precursors (blue circles and triangles; see section 4.2) and modeled precursors 2 and 3 (red triangles; see section 5.3). The black line is the linear regression for the 15 measured precursors.

Q_{Total} were computed for 15 of the 19 precursor signatures presented in Figure 8 in which there was little to no overlap of pulses, so that the charge of the first current pulse could be accurately determined. Figure 9 is a scatterplot of Q_1 versus Q_{Total} for these 15 precursors. There is a linear relationship between the two charges, with a correlation coefficient of 0.99, and the slope of the linear relationship shows that the ratio Q_1/Q_{Total} is 1.64. Figure 9 also shows the charges Q_1 and Q_{Total} that were computed for the model-predicted current signatures for precursors 2 and 3 (see section 5). Precursor 1 was not used for the calculation because its pulses overlapped, making it impossible to determine accurately the charge in the first pulse.

5. Modeling

[24] In this section, we model three representative precursor current signatures (referred to as precursors 1, 2, and 3) that occurred on the same triggering wire (UF0937) when the wire top was at heights of 205 m, 307 m, and 339 m, respectively. We begin by describing the incident current waveforms used as model input, which are inferred from the wire-base measurements. Next, we describe the distributed circuit transmission line model and the characteristic electrical parameters used to model the precursor current propagation on the triggering wire, ground lead, and ground rod, as illustrated in Figure 11, summarized in Table 1, and discussed in section 5.2. Finally, in section 5.3 the model predictions are presented and compared to the measurements.

5.1. Model Input

[25] We first discuss the shape of input current pulse and then its amplitude. Figures 10a, 10b, and 10c present the incident current pulses used as model input for precursors 1, 2 and 3, respectively. The shape of the incident current pulse is assumed to be identical to the shape of the measured precursor from time zero to the time when the second pulse begins. Then, a power law relation is fit to the smooth current decay from the first pulse peak time to the time when the second pulse begins. The input current from the time when the second pulse begins to a time 25 μs after the pulse begins is an extrapolation of the power law relation, and the last point of the input current is set equal to zero. The first pulse of the precursor signature measured at ground is the superposition of the incident wave and a reflected wave at ground, and as a result is larger in amplitude (almost twice) than the current pulse arriving at ground (and could be potentially different from the input pulse in shape, although we assume it is not) which itself is attenuated from its initial value by propagating down the wire. Thus, the assumed input current pulses were reduced in amplitude by multiplying the entire input waveform by a scaling factor. The scaling factors, given in Figure 10 and Table 1, were found through trial and error by running the model and checking the match between the amplitudes of the first measured pulse and the first model-predicted pulse.

5.2. Model Description

[26] The transmission line model [e.g., *Sadiku*, 1994, chapter 11], shown in Figure 11, consists of three interconnected sections representing the triggering wire (top), the ground lead (middle), and the ground rod (bottom). Each is considered to be a straight, vertical, and uniform transmission line with its own parameters. The transmission line sections shown in Figure 11 are implemented in PSpice (electronic circuit-simulation software) [*Herniter*, 2002] using the lumped-element lossy transmission line model "TLUMP128" [*Roychowdhury and Pederson*, 1991; *Roychowdhury et al.*, 1994]. The PSpice model predictions for propagation on the triggering wire were verified in several cases by multiplying the discrete Fourier transform of the

Table 1. Precursor Information, Triggering-Wire Transmission Line Parameters Corresponding to the Model-Predicted Precursor Signatures That Best Match the Measured Precursor Signatures, and the Amplitude Scaling Factor of the Input Current Pulse

Precursor	GPS Time	Wire-Top Height[a] (m)	Triggering-Wire Transmission Line Parameters				Measured Speed (m s^{-1})	Amplitude Scaling Factor
			R_{TW} (Ω m^{-1})	L_{TW} (μH m^{-1})	G_{TW} (μS m^{-1})	C_{TW} (pF m^{-1})		
1	21:21:24.089508	205	0.5	3.0	1.3	4.9	2.6×10^8	0.62
2	21:21:25.351162	307	0.5	3.0	1.3	4.9	2.6×10^8	0.68
3	21:21:25.940685	339	0.5	3.0	1.3	5.3	2.5×10^8	0.74

[a]The wire length is this value minus 11 m.

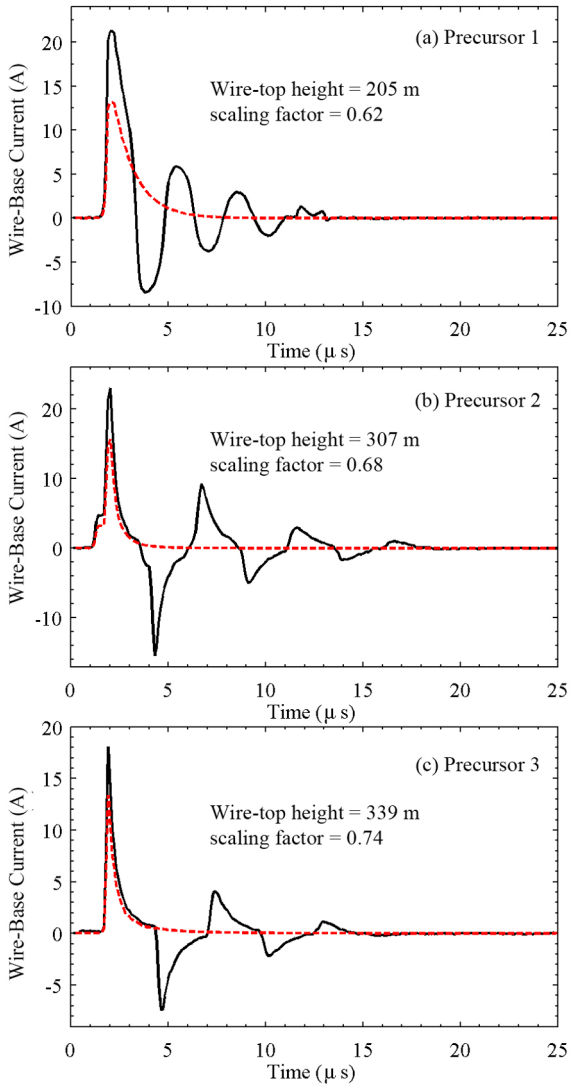

Figure 10. Incident current pulses used as inputs to the distributed circuit model shown in Figure 11 (red dashed lines) for (a) precursor 1, (b) precursor 2, and (c) precursor 3. The corresponding measurements are shown with black lines. The incident current pulses are a scaling factor smaller in amplitude than the measured initial pulses (see section 5.1).

input signal with the propagation constant (see equation (2)) in the frequency domain, and then taking the inverse discrete Fourier transform of the result. The result of the frequency domain multiplication yielded results that were identical to the time domain convolution performed by the PSpice model. The PSpice software provided a straightforward way

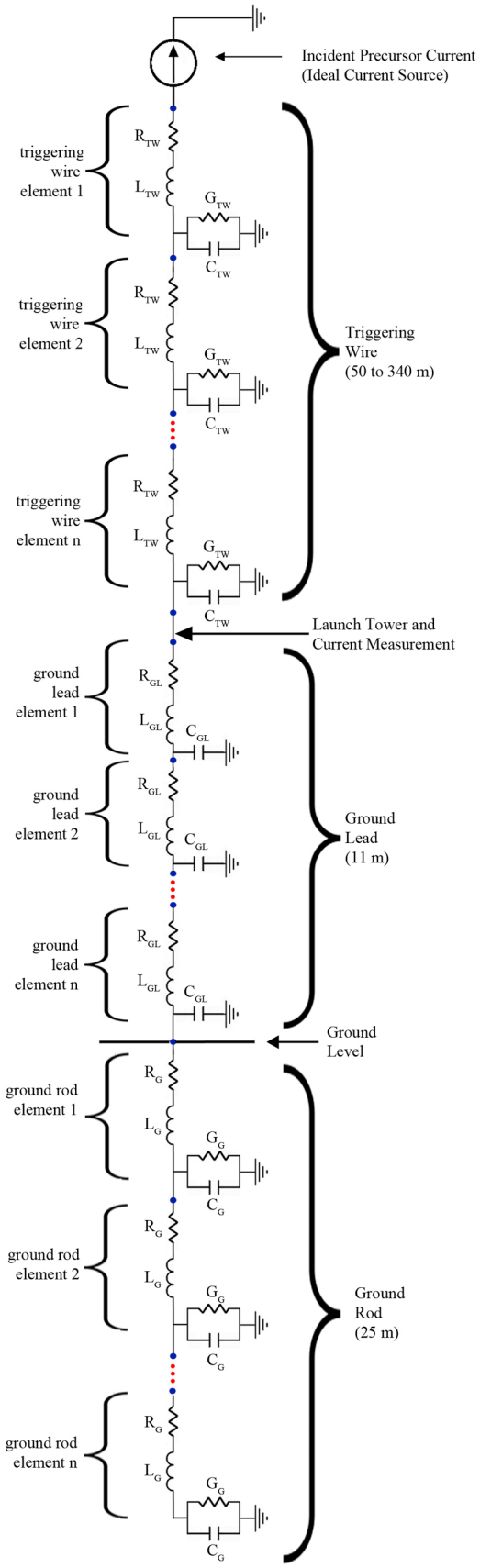

Figure 11. Distributed circuit used to model the current propagation on the triggering wire, ground lead, and ground rod. The precursor incident current is represented by an ideal current source at the triggering-wire top. In the case when the grounding impedance was assumed to be purely resistive, the ground rod distributed circuit was replaced by a resistor. Current is measured at the junction of the triggering wire and ground lead.

to connect the three transmission lines so as to be able to model the complex reflections at the transmission line connections (triggering wire to ground lead, and ground lead to ground rod). The incident precursor current pulse (at the top of the circuit in Figure 11) is input to the circuit using an ideal current source, making the current reflection coefficient at the wire tip -1. Note that the actual current measurement is made and the model output is calculated at the top of the ground lead, which is located at the bottom of the triggering wire. The model predicts essentially the same current waveform at the bottom of the ground lead as at the top of the ground lead, but slightly delayed in time (by about 40 ns).

[27] The complex sinusoidal current $I(z)e^{j\omega t}$ on the transmission lines used to represent the triggering wire, ground lead, and ground rod, with $\omega = 2\pi f$, f the frequency in Hertz, and $j = \sqrt{-1}$, is described by the wave equation in the frequency (or phasor) domain [*Sadiku*, 1994]:

$$\frac{\partial^2 I(z)}{\partial^2 z} = \gamma^2 I(z) \tag{1}$$

where z is the propagation distance, and γ is the propagation constant, defined in terms of the distributed circuit parameters as

$$\gamma = \alpha + j\beta = \sqrt{(R + j\omega L)(G + j\omega C)} \tag{2}$$

where R, L, G and C are the series resistance, series inductance, shunt conductance, and shunt capacitance, respectively, all per unit length. In equation (2), α is the attenuation constant and β is the phase constant, given by:

$$\alpha = \mathrm{Re}\{\gamma\} = \left\{ \left[RG - \omega^2 LC + \sqrt{(RG - \omega^2 LC)^2 + \omega^2 (LG + RC)^2} \right] \Big/ 2 \right\}^{1/2} \quad [\mathrm{Np\ m^{-1}}] \tag{3}$$

$$\beta = \mathrm{Im}\{\gamma\} = \left\{ \left[\omega^2 LC - RG + \sqrt{(RG - \omega^2 LC)^2 + \omega^2 (LG + RC)^2} \right] \Big/ 2 \right\}^{1/2} \quad [\mathrm{radian\ m^{-1}}]. \tag{4}$$

[28] The attenuation constant unit "Np" is a Neper, the commonly used dimensionless unit of attenuation. The transmission line characteristic impedance, the ratio of the voltage to the current for a wave traveling in the +z direction, is given by:

$$Z = \frac{\sqrt{R + j\omega L}}{\sqrt{G + j\omega C}} \quad [\Omega]. \tag{5}$$

[29] The time domain solution to the frequency domain wave equation, equation (1), for a single frequency wave propagating in the +z direction is:

$$I(z,t) = \mathrm{Re}\left\{ I_0 e^{-\gamma z} e^{j\omega t} \right\} = I_0 e^{-\alpha z} \cos(\omega t - \beta z) \quad [\mathrm{A}] \tag{6}$$

where "Re" means the real part, and I_0 is the current amplitude at z = 0 (assumed to be real). The current wave propagation speed (phase velocity) predicted by equation (1) is:

$$v_p = \frac{\omega}{\beta} \cdot [\mathrm{m\ s^{-1}}]. \tag{7}$$

[30] In the following, we describe how the values of transmission line parameters for the triggering wire, ground lead, and ground rod were determined. The triggering wire has characteristic per-unit-length values of: series resistance R_{TW} due to the finite conductivity of the copper, series inductance L_{TW} due to the magnetic flux around the wire per unit current in the wire, and shunt capacitance C_{TW} due to the charge on and around the wire (in a corona sheath) per unit voltage. For the vertical wire above ground transmission line, one can visualize the return path (the second conductor required for any transmission line) as being the ground. Such a transmission line is necessarily nonuniform, particularly near ground, with the per-unit-length values of shunt capacitance and series inductance varying with height [e.g., *Baba and Rakov*, 2003, 2005; *Theethayi and Cooray*, 2005; *Visacro and De Conti*, 2005]. However, as a simplifying approximation, it is assumed here that all transmission line parameters are constant with height and independent of frequency, some aspects of these assumptions being discussed later in this section and in section 5.3. The DC value of per unit length resistance of the 0.2 mm diameter triggering wire, R_{TW}, was measured to be 0.5 $\Omega\ \mathrm{m^{-1}}$. The measured series resistance of the triggering wire was found via the model to be insufficient to attenuate the current pulses to the extent observed in the measured precursor signatures. Additional current attenuation was provided in the model by using an effective shunt conductance per unit length G_{TW} (associated with radial leakage current). It is important to note that the G_{TW} does not represent the true physical configuration since, in reality, transverse conduction current exists only within the corona sheath, but not in the space between the outer boundary of the corona sheath and ground. The value of G_{TW} (constant with height) was chosen so that the amplitude attenuation of the signature predicted by the model matched that of the measurement. Thus, the shunt conductance should be viewed as a means to apply additional attenuation to the current pulse as it propagates on the transmission line. The inductance per unit length L_{TW} is calculated using the relation given for a vertical conductor above ground by [e.g., *Bazelyan et al.*, 1978; *Rakov*, 1998]:

$$L = \frac{\mu_0}{2\pi} \ln\left(\frac{2h}{r}\right) \quad [\mathrm{H\ m^{-1}}] \tag{8}$$

where h is the height above ground, r is the conductor radius, and μ_0 is the permeability of free space. Equation (8) describes L_{TW} as a weak function of height that varies little over the heights of interest. In our modeling, we will use $L_{TW} = 3.0\ \mu\mathrm{H\ m^{-1}}$, the value yielded by equation (8) for a 0.2 mm diameter wire for intermediate heights around 150 m.

[31] If the current pulses propagate on the triggering wire with low losses ($R \ll \omega L$ and $G \ll \omega C$), as will be shown in section 5.3 to be the case for the primary frequencies present

in the pulses, the attenuation and phase constants described in equations (3) and (4) can be approximated as:

$$\alpha = \frac{1}{2}\left(R_{TW}\sqrt{\frac{C_{TW}}{L_{TW}}} + G_{TW}\sqrt{\frac{L_{TW}}{C_{TW}}}\right) \ [\text{Np m}^{-1}] \quad (9)$$

$$\beta = \omega\sqrt{L_{TW}C_{TW}}\left[1 + \frac{1}{8}\left(\frac{G_{TW}}{\omega C_{TW}} - \frac{R_{TW}}{\omega L_{TW}}\right)^2\right] \ [\text{radians m}^{-1}]. \quad (10)$$

[32] If the squared term in the brackets of equation (10) is assumed to be zero, which is a good approximation in our case, then equation (7) becomes:

$$v_p = \frac{1}{\sqrt{L_{TW}C_{TW}}} \ [\text{m s}^{-1}] \quad (11)$$

where v_p is the current propagation speed along the wire, and L_{TW} is the per-unit-length inductance of the wire given by equation (8). The values of capacitance per unit length, C_{TW}, that are used in the modeling are inferred from equation (11) and the measured current propagation speeds from section 4.1. The inferred values of C_{TW} are larger than the values expected from the relation given by *Bazelyan et al.* [1978] for a vertical conductor of radius r at a height h above ground:

$$C = \frac{2\pi\varepsilon_0}{\ln(2h/r)} \ [\text{F m}^{-1}] \quad (12)$$

where ε_0 is the permittivity of free space. As expected, using the values of L and C given by equations (8) and (12) in place of L_{TW} and C_{TW} in equation (11) yields a propagation speed v_p = c. The C_{TW} is often viewed as being given by equation (12), but for a value of radius that is larger than the conductor (wire) radius and equal to that of the corona sheath [e.g., *Bazelyan et al.*, 1978; *Kodali et al.*, 2005]. The value of L_{TW} computed from equation (8) is unchanged by radial expansion of charge since the inductance depends on the longitudinal current, which flows primarily in the wire owing to the wire's conductivity being much higher than that of the corona envelope [*Rakov*, 2007]. The corona sheath and the current pulses' propagation speeds being lower than that of light are discussed further in section 6.

[33] We assign to the ground lead that connects the bottom of the triggering wire to the ground rod per-unit-length values of series resistance R_{GL}, series inductance L_{GL}, and shunt capacitance C_{GL}. The ground lead (2.5 cm wide copper braid) has a measured series resistance per unit length R_{GL} of 1 mΩ m^{-1}. The shape of the copper braid was somewhere between flat and cylindrical, but as a simplifying approximation we will assume it is uniformly cylindrical with an effective radius of 1.25 cm, roughly the average radius. Under this assumption, it is expected that the electric field on the ground lead surface (which we estimate to be on the order of 10^5 V m^{-1}; see section 6) is below the level necessary for corona inception. We assume that the ground lead shunt conductance is zero, and that the current propagation speed on the ground lead wire is equal to the speed of light. The per-unit-length values of series inductance and shunt capacitance for the ground lead, determined from equations (8) and (12) using h = 11 m (the upper height of the ground lead) and an effective radius of r = 1.25 $\times$ 10^{-2} m, are L_{GL} = 1.5 μH m^{-1}, and C_{GL} = 7.4 pF m^{-1}.

[34] We model the buried ground rod in two different ways: as a lumped resistor of 20 Ω, and as a 25 m long buried vertical transmission line with series resistance R_{GR}, series inductance L_{GR}, shunt capacitance C_{GR}, and shunt conductance G_{GR}. The value of series resistance R_{GR} is DC resistance for a 16 mm diameter steel rod, $\sim$8 mΩ m^{-1}. The values of L_{GR}, C_{GR}, and G_{GR} are adapted from a model used in the work of *Mata et al.* [2000] for similar ground rods at the ICLRT. The shunt conductance is the inverse of the low-frequency, low-magnitude current resistance between the ground rod and the reference ground (surrounding soil), which has been measured to be 20 Ω [*Crawford et al.*, 2001]. The per-unit-length shunt conductance was found by dividing the inverse of 20 Ω by 25 m, yielding G_{GR} = 2 mS m^{-1}. The total values of C and L of the ground rod are determined using the following relations from *Mata et al.* [2000]:

$$C = \frac{\varepsilon_r l}{18\ln(4l/d)} \times 10^{-9} \ [\text{F}] \quad (13)$$

$$L = 2l\ln\left(\frac{4l}{d}\right) \times 10^{-7} \ [\text{H}] \quad (14)$$

where l is the length of the ground rod (25 m), ε_r is the relative permittivity of the soil, which we assume is 10 [*Mata et al.*, 2000], and d is the diameter of the ground rod (16 mm). The total values of C and L for the grounding rod according to equations (13) and (14) were 1.6 nF and 44 μH, respectively. The total values of C and L were converted into per-unit-length values via division by 25 m, yielding values of L_{GR} = 1.8 μH m^{-1} and C_{GR} = 64 pF m^{-1}.

5.3. Model Results

[35] Table 1 summarizes the parameters of the triggering-wire transmission line that yielded the model predictions that best fit the measurements, the scaling factors (section 5.1) needed to match the first-pulse amplitude of the model output and measurements, the wire-top heights at which the precursors occurred, and the measured current propagation speeds on the triggering wire (see section 4.1). Figure 12 presents the three measured precursor signatures and the corresponding model predictions for the case that the grounding system is represented by a lumped resistor and for the case that the grounding system is represented by a 25 m transmission line. Figures 12 (top), 12 (middle) and 12 (bottom) each show a different precursor on a 25 μs time scale (Figure 12, left), and an expanded view from 4 μs to 9 μs (Figure 12, right). Overall, the model predictions matched better the measurements when the grounding system was represented by a 25 m transmission line than when the grounding system was represented by a lumped resistor for the following reasons: (1) the current pulse peaks in the model predictions occurred later in time, and matched better the times when the measured current pulse peaks occurred, (2) the shapes of the model-predicted current pulses were "smoother," and matched better the shapes of the measured current pulses, and (3) the current pulse

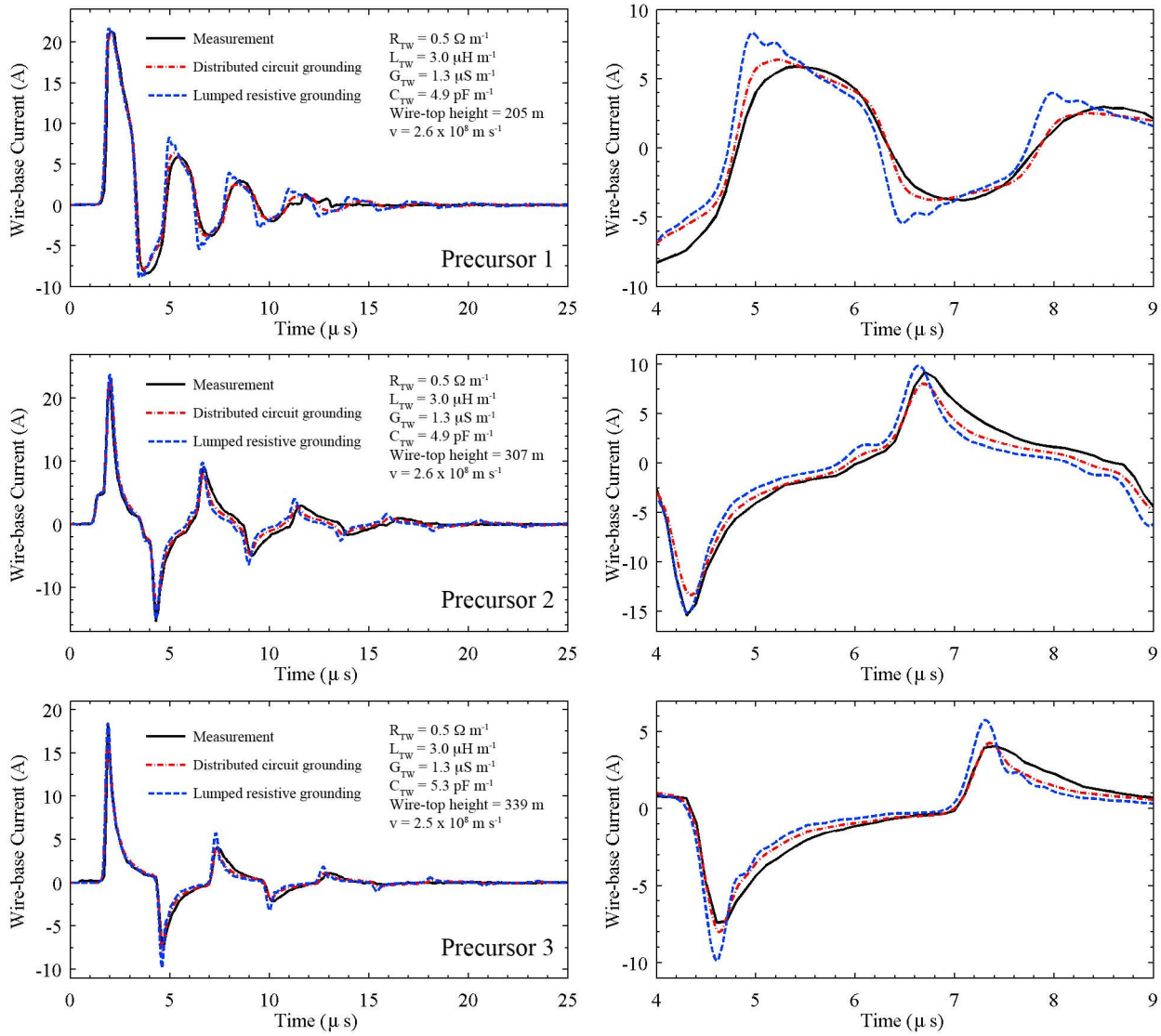

Figure 12. Measurement (solid black line) and modeling results for three precursors for two model grounding representations: when the grounding system is modeled as a 25 m distributed circuit transmission line (red dot-dashed line) and when the grounding system is modeled as a lumped resistor (blue dashed line). Precursors (top) 1, (middle) 2, and (bottom) 3 are shown on a (left) 25 μs time scale and (right) 5 μs time scale from 4 to 9 μs.

amplitudes of the model predictions matched better the measured current pulse amplitudes. For either grounding system, the model predicts that all the precursor charge eventually leaves the bottom of the triggering wire by the end of the 25 μs model run.

[36] As evident from Figure 7, the measured propagation speeds of the current pulses were lower for precursors occurring at greater wire-top heights. This observation was reproduced in the modeling by using greater triggering-wire capacitance per unit length for longer wire without increasing either the per-unit-length values of series resistance or shunt conductance. As can be seen in Table 1, the measured current propagation speed for precursors 1 and 2 was 2.6 $\times$ 10^8 m s^{-1}, and according to equation (11), the capacitance per unit length of the triggering wire, C_{TW}, for these precursors was 4.9 pF m^{-1}. The measured current propagation speed for precursor 3 was 2.5 $\times$ 10^8 m s^{-1}, or about 4% slower than the speed for precursors 1 and 2, and according to equation (11), the value of C_{TW} was 5.3 pF m^{-1}, or about 8% higher than the value of C_{TW} for precursors 1 and 2. For precursor 2, there is timing mismatch between the current pulse peaks for the model predictions and the measurement, as can be seen beginning at about 11 μs in Figure 12 for the fifth, sixth, and seventh current pulse. It is apparent that the peaks of the blue dashed line (model prediction) come before the peaks of the solid black line (measurement). The mismatch indicates that the value of C_{TW} used for precursor 2, 4.9 pF m^{-1}, was too low. Using a C_{TW} value of 5.1 pF m^{-1} in the model yields a signature with current-pulse reflection timing that matches better that of the measured current-pulse reflections.

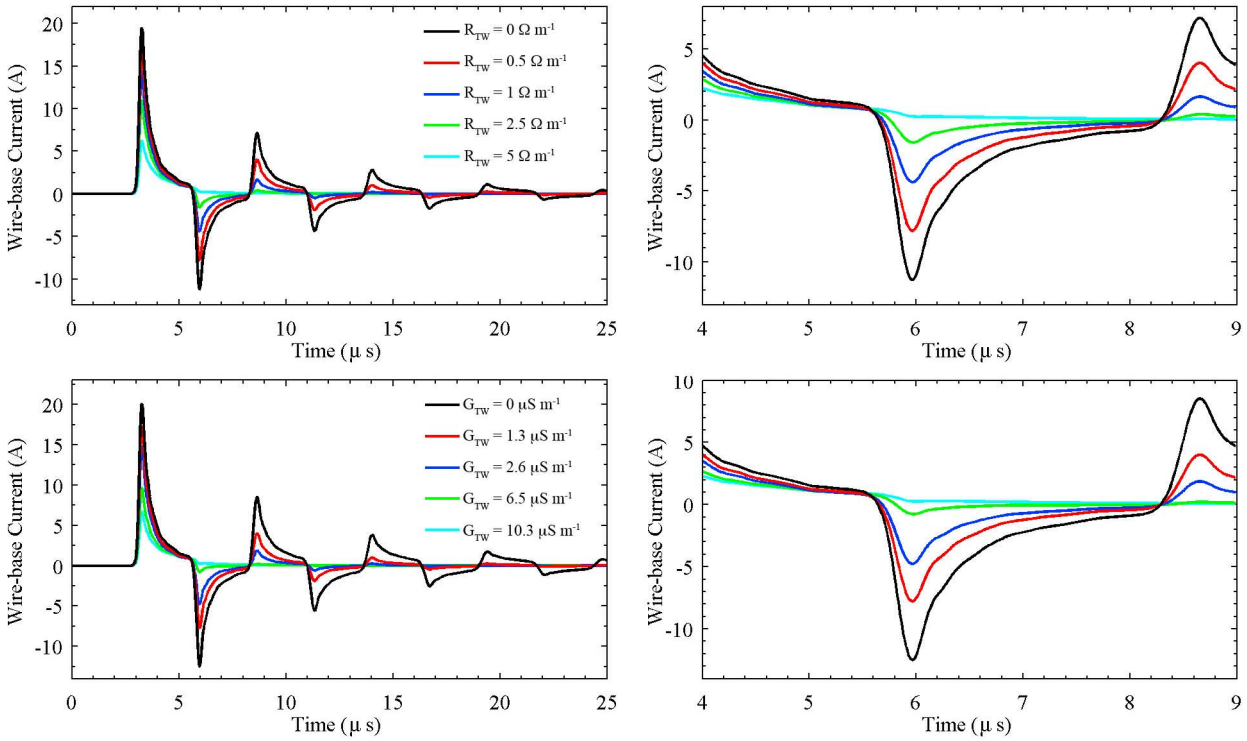

Figure 13. Model predictions for precursor 3 using the same values of R_{TW}, L_{TW}, C_{TW}, and G_{TW}, but with (top) varied values of R_{TW} and (bottom) varied values of G_{TW}. In both cases the grounding system is modeled as a 25 m transmission line. (left) Model predictions on a 25 μs time scale and (right) an expanded 5 μs time scale from 4 to 9 μs are shown. In each case, increasing values of R_{TW} or G_{TW} correspond to the curves with smaller first-peak amplitudes. Note that the measured current signature is not shown here. The red curves are the same model predictions as shown in Figure 12.

[37] A transient pulse having a full width of 3 μs, like that of the input current pulses, approximately corresponds to a primary sinusoidal wave in the Fourier spectrum having a period of 6 μs, or a frequency of about 170 kHz. The discrete Fourier transforms of the input current pulses show that nearly all of their spectral content is above this frequency. The values of R_{TW}, L_{TW}, G_{TW}, and C_{TW} for the triggering wire that yielded the best model predictions satisfy the low-loss conditions for frequency content $f \gg R_{TW}/2\pi L_{TW} \cong 30$ kHz and $f \gg G_{TW}/2\pi C_{TW} \cong 40$ kHz, so equations (9) and (10) are good approximations for the main portion of the pulse since 40 kHz is far below the frequency of 170 kHz. Clearly, however, the input current pulses contain low-frequency components that do not satisfy the low-loss criterion, and a DC component to which the transmission line theory does not apply. Low-loss restrictions were not used in the model solutions presented in Figure 12 (or Figure 13). The calculations above indicate that the primary current-pulse frequency content is sufficiently high to propagate on the triggering wire in the low-loss mode, which justifies the calculation of C_{TW} from the propagation speed using equation (11) for lossless transmission lines (in section 5.2).

[38] Further justification that the current pulses propagate on the triggering wire in the low-loss mode can be found by comparing the exact attenuation constant given by equation (3), to the low-loss attenuation constant, given by equation (9), using the characteristic values found via modeling. The attenuation constant for propagation on the triggering wire yielded by equation (3) is 8.2×10^{-4} Np m^{-1} for frequencies less than about 10 kHz, and for greater frequencies, the attenuation constant increases by less than 1% at the highest measured frequency of 3 MHz. The attenuation constant is essentially identical for the three values of C_{TW} in Table 1. The low-loss approximation for the attenuation constant yielded by equation (9), which is frequency independent, is the same, 8.2×10^{-4} Np m^{-1}. The attenuation constant value of 8.2×10^{-4} Np m^{-1} for the triggering wire was determined by comparing the model current-pulse peak amplitudes after the current pulses have traversed 25% and 75% of the triggering-wire length. The pulse peak decreases by 8% for 100 m of propagation on the triggering wire.

[39] The characteristic impedance of the triggering wire, Z_{TW}, yielded by equation (5) using the characteristic values found via modeling, is about 600 Ω for frequencies below about 10 kHz, increases for higher frequencies, and becomes constant at about 800 Ω for frequencies higher than 200 kHz. The characteristic impedance of the ground rod, Z_{GR}, is 2 Ω for frequencies below 100 Hz, and increases to about 120 Ω at a frequency of 3 MHz. If the presence of the ground lead between the triggering wire and ground rod has a negligible effect on the current entering the grounding system transmission line, as the model predicts, then the current reflection coefficient at the bottom of the triggering wire (as

though it were connected directly to the 25 m transmission line grounding impedance) is given by:

$$\Gamma_{TW-GR} = \frac{Z_{TW} - Z_{GR}}{Z_{TW} + Z_{GR}}. \quad (15)$$

[40] According to equation (15), the current reflection coefficient is slightly less than 1 at frequencies below 10 kHz, and it decreases with increasing frequencies to a value just below 0.8 at a frequency of 3 MHz. The current reflection coefficient at the bottom of the triggering wire can be inferred from the model by taking the ratio of the peak amplitude of the first upward, ground-reflected current pulse to the peak amplitude of the first downward current pulse. These two pulses overlap near the bottom of the triggering wire, so the peak amplitudes were measured in the model at the midpoint of the triggering wire, and then adjusted appropriately to account for the expected attenuation after propagating a distance equal to the triggering-wire length by multiplication with exp(-α·wire length). Doing this for precursors 1, 2 and 3 yielded an inferred current reflection coefficient at ground of about 0.9, which is in the range of values calculated using equation (15).

[41] The ratio of the amplitudes of the incident current pulse used as model input and the first current pulse measured at the wire base (the scaling factor; see section 5.1) increased with increasing wire-top height. For precursors 1, 2 and 3, the amplitude scaling factors determined by trial and error were 0.62, 0.68, and 0.74, respectively. If the current reflection coefficient at the bottom of the triggering wire is 0.9 and the attenuation constant is 8.2×10^{-4} Np m^{-1}, then the scaling factors that were used for precursors 1, 2 and 3 are approximately equal to $[(1.9)\exp(-8.2 \times 10^{-4} \times \text{wirelength})]^{-1}$. This expression yields scaling factors of 0.62, 0.67, and 0.69 for precursors 1, 2 and 3, respectively.

[42] The analysis of section 4.2 was performed on precursors 2 and 3 (precursor 1 did not meet the criterion for inclusion in the analysis because the successive pulses overlapped and the starting points of successive pulses were not distinguishable). The peak current amplitude ratios of the modeled precursors (i_2^{peak}/i_1^{peak}, i_3^{peak}/i_2^{peak}, i_4^{peak}/i_3^{peak}) are similar to those in Figure 8, ranging from 0.51 to 0.74 with an arithmetic mean of 0.62. The charges Q_1 and Q_{Total} from the modeled and measured current signatures for precursors 2 and 3 were similar (see Figure 9). The ratios of Q_1/Q_{Total} for the model-predicted signatures 2 and 3 were 1.63 and 1.47, similar to the ratios for the measured signatures, 1.62 and 1.47.

6. Discussion

[43] There is a good match between the model-predicted and measured precursor current signatures for all three representative precursors. The precursor current signatures from the distributed circuit model match better the measured precursor signatures when the grounding system is represented by a 25 m transmission line, rather than a lumped resistor. The apparent frequency dependence of the ground rod characteristic impedance may be compensating for neglected frequency dependence elsewhere in the model, such as the tendency for high-frequency currents to flow closer to the conductor surface, thereby lowering the cross-sectional area through which the current flows and increasing the effective resistance, known as the skin effect [*Sadiku*, 1994, chapter 10]. For the copper triggering wire, the skin depth (the conductor depth at which the current density is about a factor e^{-1} smaller than at the conductor surface) is equal to the wire radius (0.1 mm) at a signal frequency of about 425 kHz. As noted in section 5.3, the frequency content of the current pulses is mostly greater than 170 kHz, so the true value of R_{TW} is expected to be higher than the measured DC value, but only up to a factor of 1.6 higher at 3 MHz (the low-pass filter 3 dB point cutoff frequency of the digitizer). If the model value of R_{TW} were made higher, then the additional current pulse attenuation provided by the nonzero value of G_{TW} might not be necessary for the modeled pulse amplitudes to match the measured ones. The effect on current attenuation from using different values of R_{TW} or G_{TW} is discussed in the following paragraph.

[44] Figure 13 presents model predictions for precursor 3 when the value of either R_{TW} or G_{TW} is varied by factors of 0, 1, 2, 5 and 10, to illustrate the range of behavior that might be expected if triggering wires of different dc resistance were used, or if the value of G_{RW} were different. Figure 13 (top) shows, on different time scales, five model predictions for five values of R_{TW}: 0, 0.5, 1, 2.5 and 5 Ω m^{-1}, with L_{TW}, C_{TW} and G_{TW} being equal to the values used for the model predictions in Figure 12. Figure 13 (bottom) shows, on different time scales, five model predictions for five values of G_{TW}: 0, 1.3, 2.6, 6.5 and 13 μS m^{-1}, with L_{TW}, C_{TW} and G_{TW} equal to the values used for the model predictions in Figure 12. In all cases the grounding system is modeled as a 25 m transmission line. Note that the measurements are not shown in Figure 13. It is evident from Figure 13 that changing either R_{TW} or G_{TW} changes the amplitudes of the model-predicted current pulses, but does not noticeably change the current pulse shapes, or the times at which they occur. If the value of either R_{TW} or G_{TW} is a factor of 5 higher than the value used to obtain the model predictions in Figure 12, then the current is attenuated to essentially zero by the third reflection. If the value of either R_{TW} or G_{TW} is higher by a factor of 10, then the current is attenuated to essentially zero by the first reflection. If the value of either R_{TW} or G_{TW} is zero, then the reflections continue past the time of 25 μs to which the model calculations were made. The model predictions presented in Figure 13 show that the current propagation speed is not appreciably changed for the different values of R_{TW} or G_{TW} that produce reasonable current attenuation, or for the case that R_{TW} and G_{TW} were zero, and the observed current attenuation is a result of some other factor, such as current transmission to an extending plasma channel at the wire tip. These model results support the conclusion that the increased capacitance per unit length is responsible for the current propagation speed being less than the speed of light.

[45] The waveform measurements (and necessarily the modeling results because C_{TW} is chosen to give the measured speed) show that the current propagation speed on the triggering wire is less than the speed of light, and that the current propagation speed decreases with increasing wire-top height. A current propagation speed less than the speed

of light on a vertical conductor is likely caused by the increase in capacitance per unit length above the value for a conductor of radius r, as per equation (12), caused by the "corona sheath" necessarily present around the wire owing to the high radial fields surrounding it [*Rakov*, 2007; *Biagi et al.*, 2011]. The modeling results of *Biagi et al.* [2011] predict a substantial corona sheath extending out to about 5 m that, in the time necessary to extend a grounded triggering wire to a height of 285 m, builds up to several millicoulombs of charge with the line charge density on the order of tens of μC m^{-1} that increases with height.

[46] In the following we infer the radial electric field strength on the wire surface owing to the precursor charge on the wire, and discuss the issue of corona charge surrounding the wire owing to the precursor's radial electric field. The line charge density, ρ, on the wire from the precursor current can be estimated by dividing the precursor current by the current propagation speed. The charge density for a single current peak of 50 A traveling at 2.6×10^8 m s^{-1} is on the order of 200 nC m^{-1}, much smaller than the charge per unit length of tens of μC m^{-1} induced by the quasi-static ambient field. However, according to Gauss's law for the radial electric field E_r from a line charge density ρ, valid for the charge associated with TEM waves on transmission lines since the electrostatic equations are applicable in any plane transverse to the transmission line [e.g., *Sadiku*, 1994, chapters 4 and 11],

$$E_r = \frac{\rho}{2\pi\varepsilon_0 r} \tag{16}$$

and a line charge density of 200 nC m^{-1} can produce an electric field of 36 MV m^{-1} at the triggering wire surface, well above the threshold for corona discharge. It takes a time of about 400 ns for the current to propagate 100 m at a speed of 2.6×10^8 m s^{-1}. During a single wire traversal, the intense radial electric fields on the wire surface from the precursor charge exist for about 1 μs (for a 300 m wire-top height). If the radial corona streamers propagate at a speed of 0.1 m μs^{-1} [*Cooray*, 1993], there is little time for space charge development from precursor current electric fields. Further, whatever space charge is created, it is mitigated by the oscillating current polarity, that is, charge is deposited along the wire when the current pulse is of negative polarity, and charge is removed when the current pulse is of positive polarity. Nevertheless, there will be some deposited corona charge around the wire, with some, if not most, of it flowing back into the grounded wire. The argument above is supported by the circuit model which predicts that, for the electrical parameters determined above, all of the charge input at the top of the triggering wire leaves the bottom of the triggering wire by the end of the 25 μs model run. In the model, the charge deposited on the transmission line capacitors flows off those capacitors to ground within the 25 μs duration of the model run. If all of the precursor charge is brought to ground, it is reasonable that precursor charge can be inferred from nearby net electric field change using a point charge at the wire-tip approximation, as done in the work of *Biagi et al.* [2011]. According to equation (16) the electric field on the surface of the ground lead, with an assumed effective radius of 1.25 cm, will be about 3×10^5 V m^{-1}, below the value for electrical breakdown, 3×10^6 V m^{-1}, so the assumption that the shunt conductance per unit length for the ground lead G_{GL} is zero is a reasonable one.

[47] Finally, as noted in section 5.2, in the transmission line representation for the vertical wire above ground, the shunt capacitance and series inductance, and hence the characteristic impedance must vary with height. A nonuniform transmission line model may reproduce better some of the observed current-pulse attenuation and shape change (dispersion) owing to the distributed reflections that are expected when the characteristic impedance varies in the longitudinal direction [*Baba and Rakov*, 2005]. However, it is likely that a nonzero series resistance would still be necessary to reproduce the observed current pulse attenuation.

7. Conclusion

[48] We have presented new and detailed observations of the luminosity, wire-base current, and electric field signatures produced by precursors during the wire-extension phase of rocket-and-wire-triggered lightning. Diffuse glow luminosity or distinct leader channels up to 8 m in length were observed for 83% of the analyzed precursors, confirming that the precursor current pulses that are observed in triggering wires are due to electrical breakdown at the wire tip. The rate of precursor occurrence in different launches was found to vary considerably, from a few tens of precursors to up to 10,000. We have observed negative-polarity precursors occurring at the tips of a wire extending in electric fields indicating that predominately positive charge was overhead, supporting further efforts to trigger positive-polarity lightning with the rocket-and-wire technique. The current pulse propagation speed on the triggering wire was determined to have always been less than the speed of light, and to decrease with increasing wire length, from 2.8×10^8 m s^{-1} to 2.3×10^8 m s^{-1} for wire lengths from 80 to 340 m, respectively, a decrease of 20%.

[49] We have also modeled the propagation of current pulses on a triggering wire represented by a distributed circuit, transverse electromagnetic transmission line. The modeling indicates that the lower-than-light current propagation speed is most likely due to the increased capacitance per unit length that results from the presence of a significant corona sheath surrounding the wire, as opposed to losses associated with the series resistance and/or shunt conductance. The electrical parameters of the distributed circuit model are such that the entire charge contained in the precursor current wave is brought to ground, within 25 μs or so, as opposed to some part of it being deposited along the triggering wire for long times (>25 μs). The modeling-supported estimates of the characteristic electrical parameters of the triggering wire can be used to account for the transmission line effects present in the wire-base current signature. This will enable more accurate estimates of the charge and current injected into the triggering wire tip and more quantitative studies of the electrical breakdown at the triggering wire tip with more carefully planned future experiments.

[50] **Acknowledgments.** This research was partially supported by DARPA grants HR0011-08-1-0088 and HR0011-1-10-1-0061, by NSF grant ATM 0852869, and by NASA grant NNK10MB02P. Appreciation is owed to Julia Jordan and Mike Stapleton, who assisted in experimental setup, maintenance, and data gathering.

References

Baba, Y., and V. A. Rakov (2003), On the transmission line model for lightning return stroke representation, *Geophys. Res. Lett.*, *30*(24), 2294, doi:10.1029/2003GL018407.

Baba, Y., and V. A. Rakov (2005), On the mechanism of attenuation of current waves propagating along a vertical perfectly conducting wire above ground: Application to lightning, *IEEE Trans. Electromagn. Compat.*, *47*, 521–532, doi:10.1109/TEMC.2005.850690.

Bazelyan, E. M., B. N. Gorin, and V. I. Levitov (1978), *Physical and Engineering Foundations of Lightning Protection*, Gidrometeoizdat, St. Petersburg, Russia.

Biagi, C. J., D. M. Jordan, M. A. Uman, J. D. Hill, W. H. Beasley, and J. Howard (2009), High-speed video observations of rocket-and-wire initiated lightning, *Geophys. Res. Lett.*, *36*, L15801, doi:10.1029/2009GL038525.

Biagi, C. J., M. A. Uman, J. Gopalakrishnan, J. D. Hill, V. A. Rakov, T. Ngin, and D. M. Jordan (2011), Determination of the electric field intensity and space charge density versus height prior to triggered lightning, *J. Geophys. Res.*, *116*, D15201, doi:10.1029/2011JD015710.

Cooray, V. (1993), A model for subsequent return strokes, *J. Electrost.*, *30*, 343–354, doi:10.1016/0304-3886(93)90088-O.

Crawford, D. E., V. A. Rakov, M. A. Uman, G. H. Schnetzer, K. J. Rambo, M. V. Stapleton, and R. J. Fisher (2001), The close lightning electromagnetic environment: Dart-leader electric field change versus distance, *J. Geophys. Res.*, *106*, 14,909–14,917.

Herniter, M. E. (2002), *Schematic Capture With Cadence PSpice*, Prentice Hall, Upper Saddle River, N. J.

Horii, K. (1982), Experiment of artificial lightning triggered with rocket, *Mem. Fac. Eng. Nagoya Univ.*, *34*(1), 77–112.

Jerauld, J. (2007), Properties of natural cloud-to-ground lightning inferred from multiple-station measurements of close electric and magnetic fields and field derivatives, PhD dissertation, Univ. of Fla., Gainesville. [Available at http://purl.fcla.edu/fcla/etd/UFE0021279.]

Kodali, V., V. A. Rakov, M. A. Uman, K. J. Rambo, G. H. Schnetzer, J. Schoene, and J. Jerauld (2005), Triggered lightning properties inferred from measured currents and very close electric fields, *Atmos. Res.*, *75*, 335–376.

Lalande, P., A. Bondiou-Clergerie, P. Laroche, A. Eybert-Berard, J.-P. Berlandis, B. Bador, A. Bonamy, M. A. Uman, and V. A. Rakov (1998), Leader properties determined with triggered lightning techniques, *J. Geophys. Res.*, *103*, 14,109–14,115, doi:10.1029/97JD02492.

Laroche, P., A. Eybert-Berard, L. Barret, and J. P. Berlandis (1988), Observations of preliminary discharges initiating flashes triggered by the rocket and wire technique, paper presented at the 8th International Conference on Atmospheric Electricity, Int. Comm. on Atmos. Electr., Uppsala, Sweden.

Mata, C. T., M. I. Fernandez, V. A. Rakov, and M. A. Uman (2000), EMTP modeling of a triggered-lightning strike to the phase conductor of an overhead distribution line, *IEEE Trans. Power Delivery*, *15*, 1175–1181, doi:10.1109/61.891499.

Rakov, V. A. (1998), Some inferences on the propagation mechanisms of dart leaders and return strokes, *J. Geophys. Res.*, *103*, 1879–1887.

Rakov, V. A. (2007), Lightning return stroke speed, *J. Lightning Res.*, *1*, 80–89.

Roychowdhury, J. S., and D. O. Pederson (1991), Efficient transient simulation of lossy interconnect, paper presented at 28th Design Automation Conference, Assoc. for Comput. Mech., Int. Electr. and Electron. Eng., San Francisco, Calif.

Roychowdhury, J. S., A. R. Newton, and D. O. Pederson (1994), Algorithms for the transient simulation of lossy transmission lines, *IEEE Trans. Comput. Aided Design Integrated Circuits Syst.*, *13*, 96–104.

Sadiku, M. N. O. (1994), *Elements of Electromagnetics*, Saunders Coll., Orlando, Fla.

Theethayi, N., and V. Cooray (2005), On the representation of the lightning return stroke as a current pulse propagating along a transmission line, *IEEE Trans. Power Delivery*, *20*, 823–837, doi:10.1109/TPWRD.2004.839188.

Visacro, S., and A. De Conti (2005), A distributed-circuit return-stroke model allowing time and height parameter variation to match lightning electromagnetic field waveform signatures, *Geophys. Res. Lett.*, *32*, L23805, doi:10.1029/2005GL024336.

Willett, J. C., D. A. Davis, and P. Laroche (1999), An experimental study of positive leaders initiating rocket-triggered lightning, *Atmos. Res.*, *51*, 189–219, doi:10.1016/S0169-8095(99)00008-3.

C. J. Biagi, J. D. Hill, D. M. Jordan, V. A. Rakov, and M. A. Uman, Department of Electrical and Computer Engineering, University of Florida, Gainesville, FL 32611, USA. (biagi@ufl.edu)